THE USE OF RARE EARTH METALS IN Al–Si–Cu CASTING ALLOYS

M. G. Mahmoud

Mechanical Design and Production Department, Cairo University, Cairo, Egypt

Y. Zedan and V. Songmene

École de technologie supérieure, Université du Québec, Montréal, QC, Canada

A. M. Samuel and F. H. Samuel

Département des Sciences appliquées, Université du Québec à Chicoutimi, Chicoutimi, QC, Canada

Abstract

In the current study, a series of forty-two cast Al–Si–Cu–Mg -based alloys with additions of transition metals (V, Cr, Ni) and rare earth (RE) metals (La, Ce) were prepared and mechanically tested in the as-cast, T5, T6 and T7 heat treatment conditions. The microstructures were investigated using optical microscopy, scanning electron microscopy (SEM) and electron probe microanalysis (EPMA). The volume fraction, aspect ratio, and roundness of second phase constituents were determined by ImageJ analysis software. The microstructural observations show that the RE elements have a greater impact on the microstructure of cast alloys, resulting in the formation of new types of intermetallic phases containing RE, Al–Si–Cu–RE and Al–Ti–RE. With regard to the mechanical properties, it was found that the highest strength of the casting alloys was found with 0–0.2 wt% addition of Ce/La. However, the addition of more than 0.2 wt% induced a detrimental effect on the mechanical properties due to precipitation of a high volume fraction of insoluble intermetallic compounds containing RE. Excessive addition of RE elements leads to the formation of a coarse intermetallic compound along the grain boundary. Besides, RE elements have a marginal modification effect in terms of changing the morphology of the eutectic Si particles.

Keywords: Al alloys, rare earth metals, transition metals, microstructure, tensile properties

Introduction

A number of scientific investigations are reported in the literature on the effects of rare earth elements and mischmetal (MM), which is a mixture of RE elements found in abundance in nature with cerium (Ce) and lanthanum (La) together comprising approximately 90% of mischmetal. The RE metals investigated include yttrium (Y), erbium (Er), neodymium (Nd), ytterbium (Yb), samarium (Sm), scandium (Sc), europium (Eu) and gadolinium (Gd).[1–42] Among these, studies on the effects of MM, Ce, La and mixture additions of Ce and La were included in the present work.[43–54]

The influence of mischmetal, cooling rate and heat treatment on the hardness and microstructural observation of unmodified and Sr-modified A319.1, A356.2 and A413.1 Al-Si casting alloys was investigated by El Sebaie et al.[55–58] From these studies, the authors noted the following: in general, the hardness measurements revealed that the hardness values of the as-cast alloys were higher at high cooling rates than at low cooling rates. With addition of MM, the hardness decreased at both cooling rates.[59] The addition of MM to the non-modified as-cast alloys partially modified the eutectic silicon particles. This effect was more pronounced in the A413.1 and A319.1 alloys, compared to A356.2 alloy.[60] The effect of MM as a modifier is more effective at high cooling rate (corresponding to dendrite arm spacing (DAS) $\sim$ 40 μm) than at the low cooling rate (DAS $\sim$ 120 μm) for all the as-cast non-modified alloys.[60] MM-containing intermetallic phases were observed at high and low cooling rates, each exhibiting a specific Ce/La ratio and morphology. In Sr-modified alloys, many of these

MM-containing intermetallic phases were found to contain Sr, which confirmed the interaction of MM with Sr.[61]

Effects of different levels of additions (0.0–1.0 wt%) of La-based MM and heat treatment on the microstructure and tensile properties of two different sections of Al-Si casting alloy A357 were examined by Mousavi et al.[62] The results showed that optimum levels of MM additions are 0.1 wt% and 0.3 wt% for thin and thick sections of the casting, respectively. Examination of the microstructure characterization showed that at high level of addition, a new AlSiLa intermetallic phase was detected. In addition, the results demonstrated that T6 heat treatment improved the tensile properties of the Sr-modified alloys.

The cooling rate sensitivity of AlTiB grain refiner, MM and AlTiB-MM additions and the resultant effects on the microstructure and mechanical properties of A356 alloy were studied by Zhang et al.[63] Their results demonstrated that the AlTiB-MM addition provided the most effective and synergetic refinement compared to the individual AlTiB or MM additions. In addition, the properties of A356 alloy wheel refined by the AlTiB-MM addition were improved significantly. The tensile strength, yield strength and elongation of the wheel spokes improved by approximately 11.3%, 10.8% and 44.1%, respectively.

Tsai et al.[60] analyzed the modification effect of different levels of Ce on the microstructure, thermal analysis and mechanical properties of cast A356 aluminum alloys. They reported that A356 alloy modified with 1.0 wt% Ce greatly improved eutectic silicon modification; however, the thermal analysis revealed that there is no direct relation between the eutectic growth temperature and silicon modification. The microstructural characterization showed that two kinds of Ce-containing intermetallic phases were found, including Ce–23Al–22Si and Al–17Ce–12Ti–2Si–2Mg (in wt%). While the ductility of the Ce-modified alloys was enhanced for Ce additions of 0.4 wt% and above, there was no positive effect on the ultimate tensile strength, which was attributed to the formation of the Al–17Ce–12Ti–2Si–2Mg phase which reduced the amount of free Mg available for precipitation of the Mg_2Si strengthening phase.

According to Ouyang et al.,[63] addition of La to hypereutectic Al–Si alloys can enhance the effect of phosphorus on the modification of the primary Si phase, and the higher the La content at the Al–Si interface, the smaller the primary Si particle size obtained. In another research, the influence of different amounts of La on the microstructure and mechanical properties of A356 alloys was investigated by Tsai et al.[64] Their findings indicated that the modification efficiency with respect to the microstructures and mechanical properties obtained with 1.0 wt% La is similar to those observed with the use of 0.01 wt% Sr. Furthermore, the results of thermal analysis revealed that there is no direct relationship between eutectic growth temperature and silicon morphology/modification rating.

Previous studies carried out by the TAMLA research group at UQAC have investigated the influence of rare earth

Table 1. Nominal Compositions of the Present Alloys

Alloy	Composition (wt%)										
	Cu	Si	Mg	Fe	Mn	Ti	Zr	V	Ni	Sr	Cr
D00*	2.1	7.8	0.43	0.45	0.43	0.15	0	0	0	0	0
D11*	2.6	8.4	0.38	0.42	0.42	0.12	0.15	0.2	0.32	0	0
D22*	2.2	7.6	0.37	0.43	0.38	0.17	0.15	0.2	1.03	0.015	0.2
B00**	2.4	1.2	0.37	0.4	0.37	0.15	0	0	0	0	0

*Base alloys (high Si%), **low Si%—reference alloy
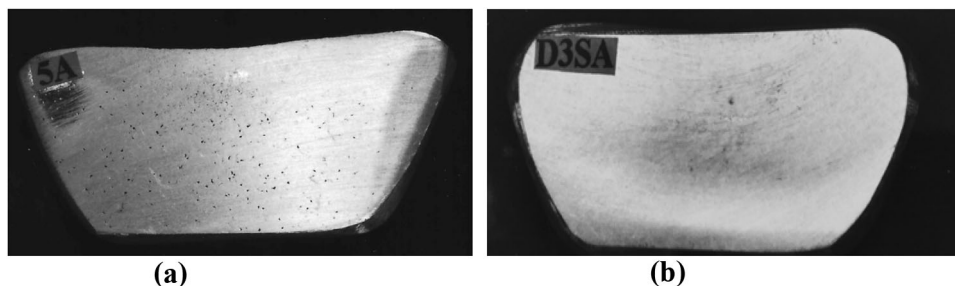
Figure 1. Porosity distribution: (a) before degassing, (b) after degassing.

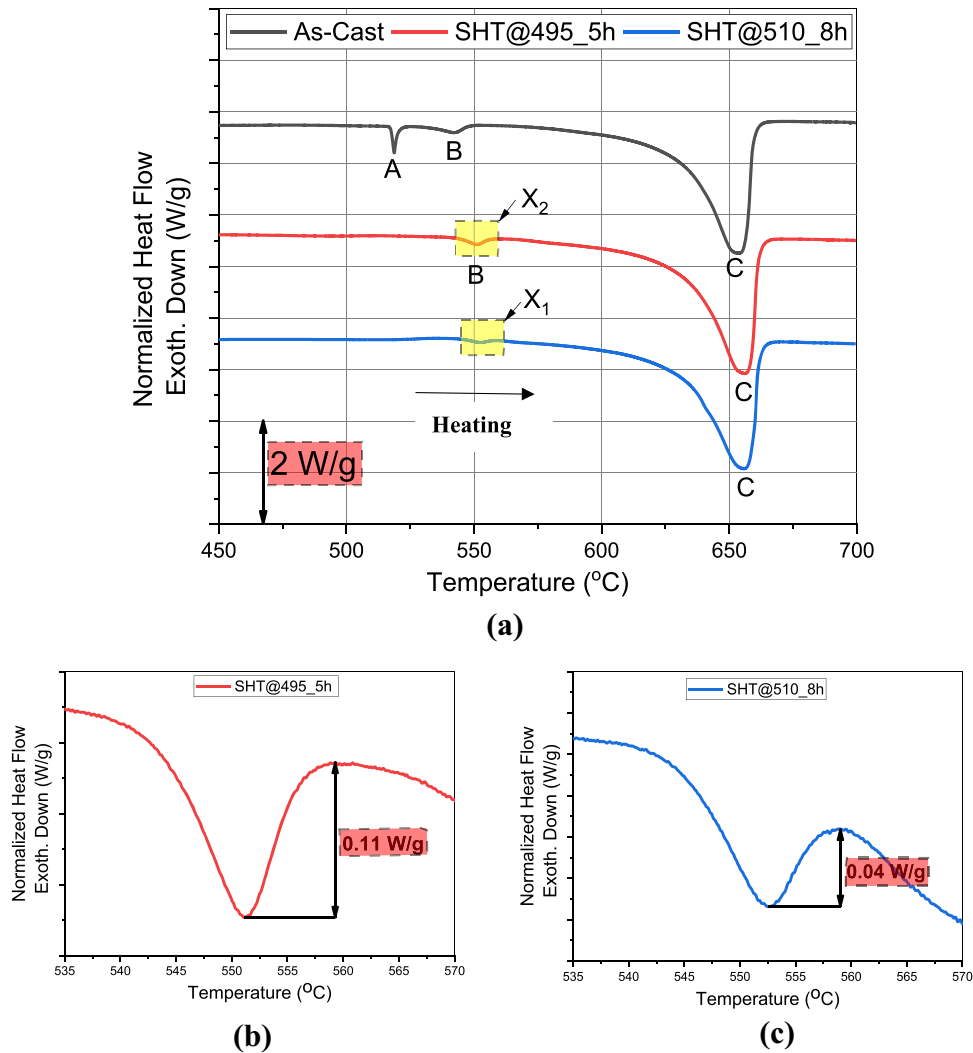| Heat treatment condition	Solution temperature, (°C)	ST holding time, (h)	Quenching temperature (°C)	Aging temperature (°C)	Aging time (h)
SHT	510	8	70	None	None
T5	None	None	None	180	8
T6	510	8	70	180	8
T7	510	8	70	240	4

Figure 2. (a) DSC melting curves of D00 alloy in the as-cast and different solution heat-treated (SHT) conditions, (b, c) enlarged portions of (Al-Cu) reaction in (a) marked X2 and X1, respectively.

elements and mischmetal on the performance of A356, A413.1 and other Al–Si alloys.[65–71] With the more recent focus on the development of new Al–Cu-based alloys for high-temperature performance of automotive components, it was considered worthwhile to also investigate the effects of Ce and La rare earth metal additions to these alloys, taking into consideration low 1.2% Si alloy (coded B00

reference alloy for Si effect) and relatively high Si (8%Si coded D00) levels.

The present article focuses on the addition of individual role of high-purity La and Ce, up to 1% each, on the microstructure and room temperature tensile properties of transition metals-containing Al–Si–Cu–Mg–X-based alloy, where X = Ti, V, Mn, Fe, Ni, Sr. It is worth mentioning
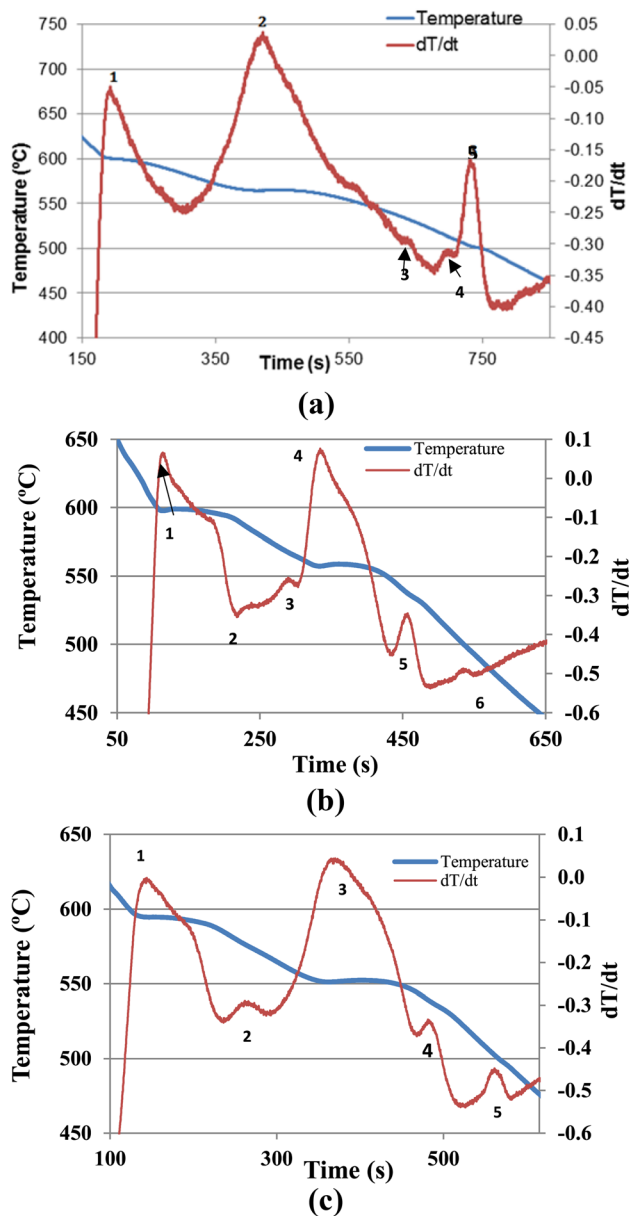
Figure 3. Temperature–time curves obtained from: (a) D00, (b) D00 + 5%Ce, (c) D00 + 5%La.

here that the present D00 alloy is a modified version of B319 alloy with 2.5% higher Si, 1% lower Cu and a high Mn content (0.6%) to insure the precipitation of all Fe-intermetallics in the form of α-Al_{15}(Fe, Mn)$_3$Si$_2$ Chinese script instead of β-Al_5FeSi. As a result, the new alloy should have a better fluidity than the B319 alloy and hence provide sounder castings. In other words, it falls between B319 and 332 alloys.

Experimental Procedure

The as-received alloy was grain-refined using Al–5%Ti–1%B master alloy to achieve a Ti level of 0.15 wt%. Other alloys were prepared from this grain-refined alloy,

considered as the base alloy, by adding Sr, Ni, Zr, V, Cr, La and Ce to the base Al–8%S–2.5%Cu–0.45%Mg–0.45%Fe–0.65%Mn alloy melt. Table 1 shows the details of the additions made in each case. Both La and Ce were added to each alloy (D00, D11, and D22) at three different concentrations, viz. 0.2%, 0.5% and 1%. All of the alloys were mechanically tested in order to acquire an understanding of the effects of these additives on their tensile properties. Rare earth elements Ce and La of high purity (99.7%) were supplied by Stanford Advanced Materials, USA.[72] As for the other elements, they were added in the form of commercial master alloys, i.e., Al–10% Sr, Al–20% Ni, Al–15% Zr, Al–25% V, Al–25% Cr. Alloys so prepared were classified based on the Si content, and the Ce and La addition levels made as listed in Table 1.

The raw material ingots were cut into smaller pieces and melted in a 40-Kg-capacity SiC crucible, using an electrical resistance furnace. The melting temperature was maintained at 750 ± 5 °C. All alloys prepared were grain-refined using Al–5% Ti–1% B to obtain levels of 0.15 wt% Ti. Additions of La and Ce rare earth metals were made in amounts of 0.2, 0.5 and 1.0 wt% using Al–15% La and Al–15%Ce master alloys. For purposes of comparison with modification with RE, individual addition of 150 ppm Sr was also made to one of the base alloys (coded D22). In each case, the melts were degassed for 15–20 min employing a graphite impeller rotating at 130 rpm, using pure dry argon, and then the melt was carefully skimmed to remove oxide layers from the surface before casting-humidity was less than 15%. Strontium was added only 5 min before the end of degassing to reduce the possibility to its oxidation. Prior to pouring, samples were examined using reduced pressure test (RPT) for porosity formation, as shown in Figure 1.

The melt was poured into an ASTM B-108 permanent mold (coated with boron nitride and preheated at 450 °C to drive out moisture), for preparing the tensile test bar castings. Each casting provides two test bars, with a gauge length of 70 mm and a cross-sectional diameter of 12.7 mm. Three samplings for chemical analysis were also taken simultaneously at the time of the casting; this was done at the beginning, in the middle, and at the end of the casting process to ascertain the exact chemical composition of each alloy. The chemical analysis was carried out using a Spectrolab-JrCCD Spark Analyzer.

For the purpose of determining the reactions taking place during solidification, part of the molten metal was also poured into an 800-g-capacity graphite mold preheated to 650 °C so as to obtain close-to-equilibrium solidification conditions at a solidification rate of 0.35°C/s. A high sensitivity Type-K (chromel-alumel) thermocouple, which has to be insulated using a double-holed ceramic tube, is attached to the center of the graphite mold. The temperature–time data are collected using a high-speed data

Table 3. Description of Phases Deduced from Figure 2

Figure #	Reaction #	Temperature (°C)	Suggested phase[73]	Freezing zone (°C)
2a	1	600	Formation of α-Al dendritic network	32
	2	570	Eutectic reaction (eutectic Si + α-Fe)	
	3	538	Precipitation of Mg_2Si + π phase	
	4	515	Precipitation of $Q-Al_5Mg_8Si_6Cu_2$	
	5	500	Precipitation of $θ-Al_2Cu$ and $Q-Al_5Mg_8Si_6Cu_2$	
2b	1	600	Formation of α-Al dendritic network	42
	2	585	Precipitation of α-Fe	
	3	569	Ce-rich phase	
	4	558	Eutectic reaction (eutectic Si + α-Fe)	
	5	538	Precipitation of Mg_2Si + π phase	
	6	497	Precipitation of $θ-Al_2Cu$ and $Q-Al_5Mg_8Si_6Cu_2$	
2c	1	596	Formation of α-Al dendritic network	46
	2	575	La-rich phase	
	3	550	Eutectic reaction (eutectic Si + α-Fe)	
	4	537	Precipitation of Mg_2Si + π phase	
	5	500	Precipitation of $θ-Al_2Cu$ and $Q-Al_5Mg_8Si_6Cu_2$	

acquisition system linked to a computer system to record the temperature–time data every 0.1 second. From these data, the cooling curves and the corresponding first derivative curves for a number of selected alloys were plotted so as to identify the main reactions occurring during solidification with the corresponding temperatures, and the various phases which constitute the microstructure of each alloy are expected to be revealed as well.

A PerkinElmer DSC8000 differential scanning calorimeter operating under a protective atmosphere of pure argon was used to study the solidification behavior of the alloys used in the current study. The mass of the DSC sample was approximately 20 mg. The scans were performed in three stages as follows: (1) heating from 400 to 700 °C at a heating rate of 10 °C/min, (2) holding at 700 °C for 1 min and (3) cooling from 700 to 400 °C at a cooling rate of 10 °C/min. Three samples were tested for each alloy condition, and the results were found to be almost identical. The corrected DSC curve of each sample was determined by subtracting the two DSC scans. The first scan was conducted with the sample, while the second one was conducted without the sample under the same testing conditions of the sample scan. The purpose of this procedure was to obtain baseline-corrected thermogram data. The DSC curve of each alloy condition was subsequently obtained by averaging the three corrected curves of the three respective samples where the uncertainty in determining the peak temperatures did not exceed ± 2 °C. The peaks reported in the DSC runs were supported by thermal analysis at a very slow solidification rate ($\sim$ 0.8 °C/s).

The tensile test bars were subjected to solution heat treatment (SHT), as well as T5, T6 and T7 heat treatments (see Table 2). Tensile bars were tested at ambient temperature (25 °C) in the as-cast, solution heat-treated (SHT), and T5, T6 and T7 heat-treated conditions using an MTS Servo-hydraulic mechanical testing machine, at a strain rate of 4×10^{-4} s^{-1}.

A JEOL JSM-6480LV scanning electron microscope coupled with an energy-dispersive X-ray spectrometer (EDS) was used for examining the microstructures and semi-quantitative analysis of the phases observed using EDS, measuring the volume fraction of intermetallic phases formed, as well as examining the fracture surfaces of the tensile-tested alloy samples. A JEOL JXA-8900 electron probe microanalyzer (EPMA), equipped with a wavelength-dispersive spectrometer (WDS), was also employed for examining the microstructures and identification of the new intermetallic phases formed.

Results and Discussion

Solidification and Microstructural Characterization

The main objective of this step was to examine the effect of different solution heat treatments on the dissolution of the low-melting-point Cu-rich phases. As it may be noted from Figure 2, after solutionizing at 495 °C, the disappearance of peak A indicates the dissolution of the eutectic Al_2Cu and $Q-Al_5Mg_8Si_6Cu_2$ phases. The height of peak B was also decreased compared to the as-cast condition,
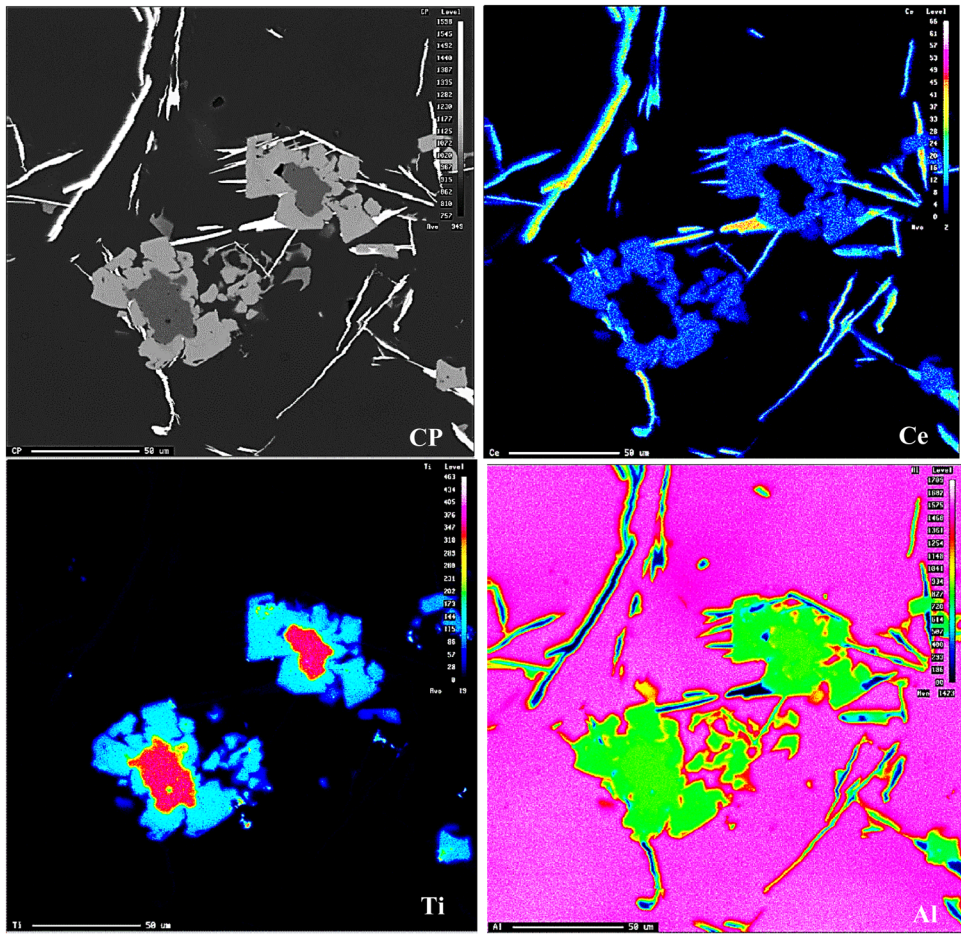
Figure 4. Precipitation of Ce-rich phase particles on the pre-existing Al₃Ti particles.

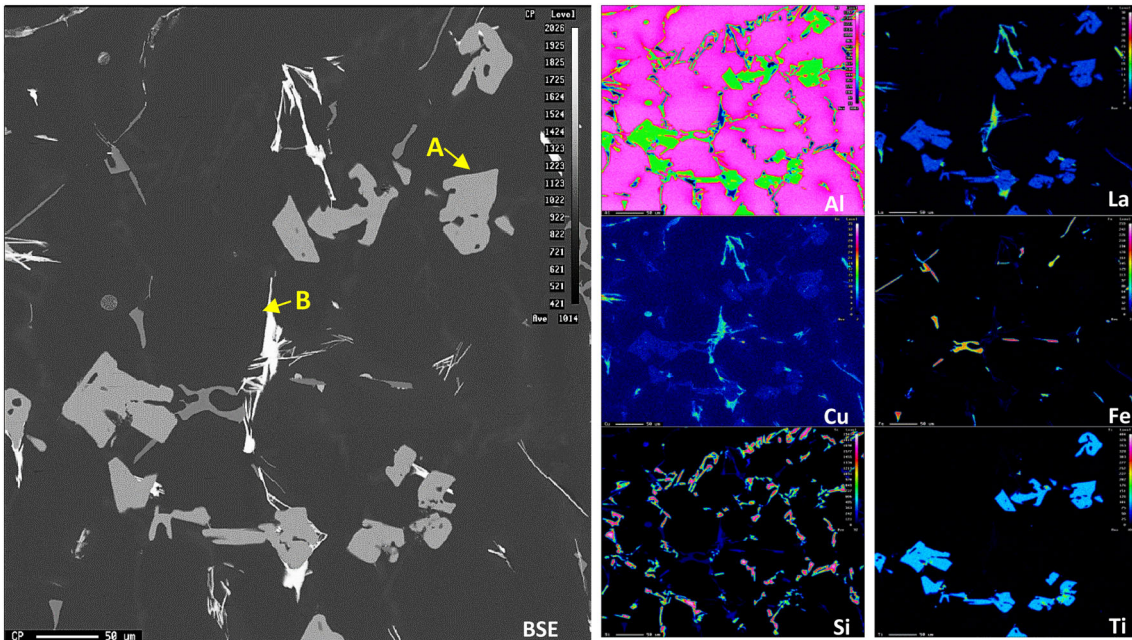**Figure 5. Backscattered electron image of as-cast D00 alloy with 1.0 wt% La addition and corresponding X-ray images of Al, La, Cu, Fe, Si and Ti.**

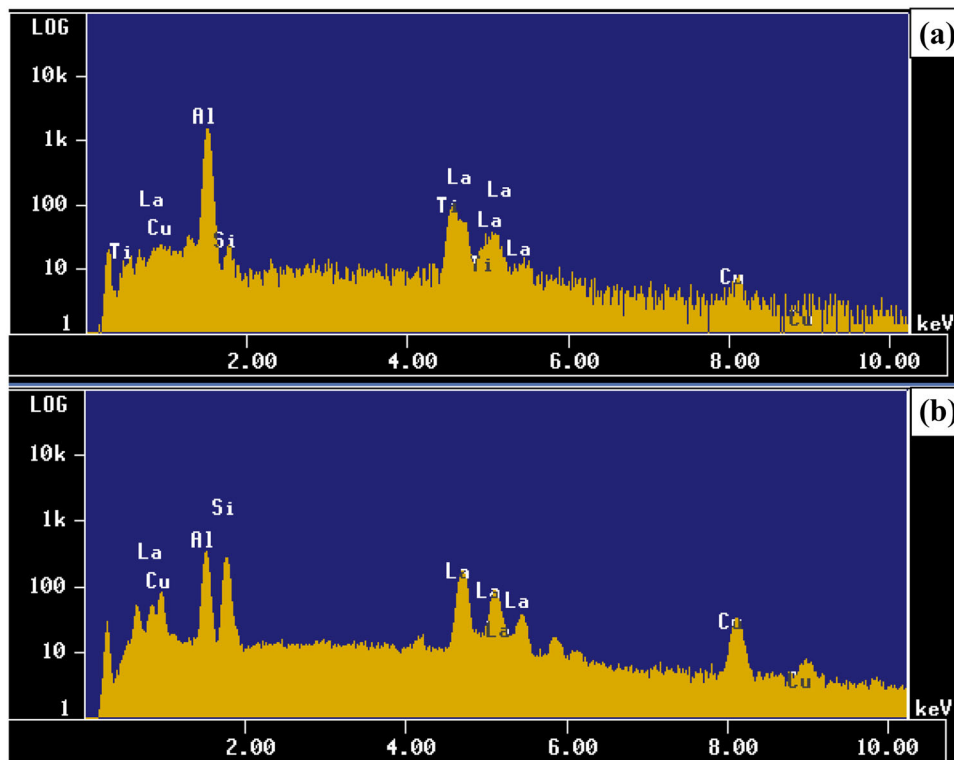**Figure 6.** EDS spectra of locations marked A and B in Figure 5 corresponding to: (a) gray phase and (b) white phase.

indicating that the blocky Al_2Cu phase was partially dissolved. Increasing the temperature or the time of the solution treatment further decreased the height of peak B. Based on these observations, after solution heat treatment at 510 °C for 8 h, peak A was completely dissolved for D00 alloy (X_1 in Figure 2c).

In order to identify the precipitation temperature of RE-phases, the amounts of added Ce and La were increased to 5% each. Figure 3 shows a series of solidification curves and their first derivatives obtained from thermal analysis, whereas Table 3 summarizes the expected reactions.

Table 3 reveals that the RE-rich intermetallics precipitate in the mushy zone at temperatures of 569 °C and 575 °C, for Ce- and La-containing intermetallic phases, respectively. Apparently the addition of 5% of Ce or La resulted in increasing the freezing zone from 30 °C (base alloy D00) to 42 °C (alloy D00 + 5%Ce) or 46 °C (alloy D00 + 5%La). The presence of Al_3Ti particles in the melt enhanced the precipitation of RE-based intermetallics as shown in Figure 4 where the Al_3Ti particle is seen at the center of the precipitated Ce-rich particles. As mentioned previously, the depression in the eutectic temperature from 570 °C (base alloy) to 550 °C (base alloy + 5%La) has no reflection on the morphology of the eutectic Si particles.

The addition of RE to alloy D00 resulted in the formation of two different intermetallic phases, colored white and gray in the backscattered electron (BSE) images shown in Figure 5. Based on the EDS analysis, these phases are Al–Si–Cu–RE (Ce/La) and Al–Ti–RE (Ce/La), respectively—Figure 6. This observation is ascribed to the high Si level (8.0 wt%) in D00 alloy in addition to the high RE additions (1.0 wt%), where the Si, Al, and Cu interact with the RE (Ce/La) to form the white phase with different chemical compositions.[65]

The BSE images obtained from as-cast samples of D00 alloys containing 1.0 wt% La and Ce additions are shown in Figure 7. The results show that both La and Ce are found to have the same effect on the microstructures, with the La- and Ce-containing intermetallics also displaying similar morphologies. Figure 7 reveals that RE(Ce/La) addition of 1.0 wt%, increases the relative amount of intermetallic particles. In addition, these images also reveal that these RE intermetallic compounds were observed to precipitate within the inter-dendritic regions.

With regard to the La-containing alloys, Figure 8 compares the optical micrographs of D00 alloy containing 0.2 wt% La in as-cast and solution heat-treated (SHT) conditions. It can be observed that the acicular eutectic silicon particles in D00 base alloy in Figure 8a partially transform into finer and more spherical particles with the addition of 0.2 wt% La (white circle). This observation is in contrast to the results reported by Yi and Zhang[74] who noted simultaneous modification of both primary and eutectic Si particles is
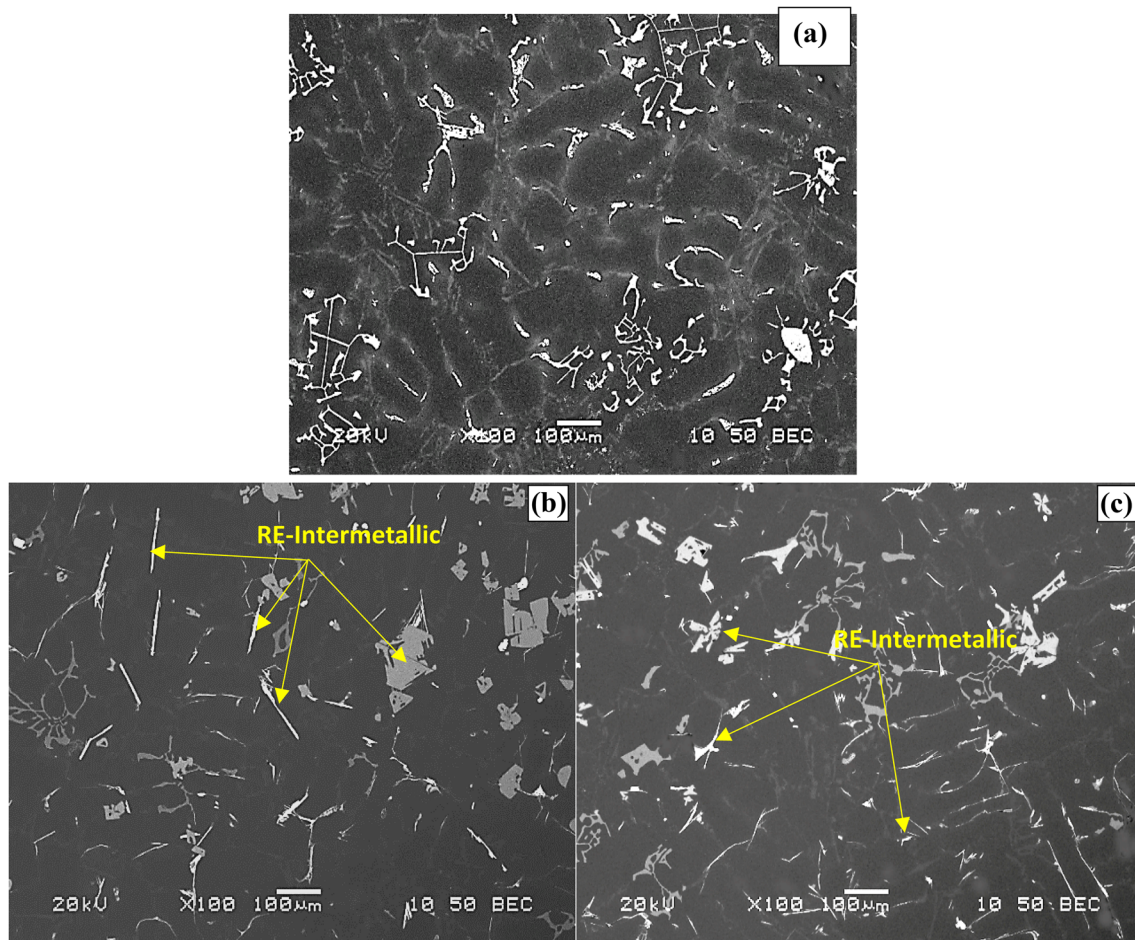
Figure 7. Backscattered electron images of as-cast D00 alloys containing (a) 0.0 wt% RE, (b) 1.0 wt% Ce and (c) 1.0 wt% La.

obtained with the addition of pure La to hypereutectic Al–17% Si alloys and that the optimal modification effect is achieved at 3.3 wt% La. As in the case of La addition, the La-rich intermetallic phases are also observed in both the as-cast and solution heat-treated D00 alloy samples, as seen in Figure 8a, b, c indicating the insoluble nature of the La-based intermetallic phase. However, the high magnification image presented in Figure 8b reveals the possibility of fragmentation of RE-based intermetallics as indicated by the perforated platelet (arrowed). Figure 8d obtained from D22 alloy in the as-cast condition reveals complete modification of the eutectic Si particles. Figure 8e, f shows the precipitation of dense amount of Al_2Cu when the D00 alloy was heat-treated in T6 condition, whereas Figure 8f reveals the size of the precipitated particles varies between 10 and 40 nm.

Tensile Properties

Tensile tests were carried out on test bars of the B00 and D00 alloys to study the effect of solution heat treatment parameters (temperature and time) on the tensile properties (UTS, YS and %El), in order to support the DSC results. It

may be seen from Figure 9 that the results obtained from the tensile tests are in accordance with the DSC results, where the alloys solution-treated at 510 °C for 8 h exhibited better properties than those that were solution-treated at 495 °C for 5 h. When the solution treatment changes from 510 °C for 8 h to 495 °C for 5 h, this leads to an increase in the UTS and YS of B00 alloy from 324 to 349 MPa and 278 to 348 MPa, respectively, with a negligible drop in ductility from 2.28 to 2.17%, as shown in Figure 9, whereas for D00 alloy, the strength values increase from 357 to 382 MPa (UTS) and from 346 to 361 MPa (YS), with a small increase in the %El from 0.85 to 0.97%. Based on these results, the solution heat treatment of 510 °C for 8 h was applied to all the samples tested in the current study.

Figures 10 and 11 show the effects of the addition of various amounts of Ce and La on the room temperature tensile properties (UTS, YS and %El) of the base alloys corresponding to various heat treatment conditions. It is inferred from Figure 10 that the values of UTS, YS and % El of the as-cast D00 base alloy are 300 MPa, 224 MPa and 1.7%, respectively. In addition, Figure 10 reveals that
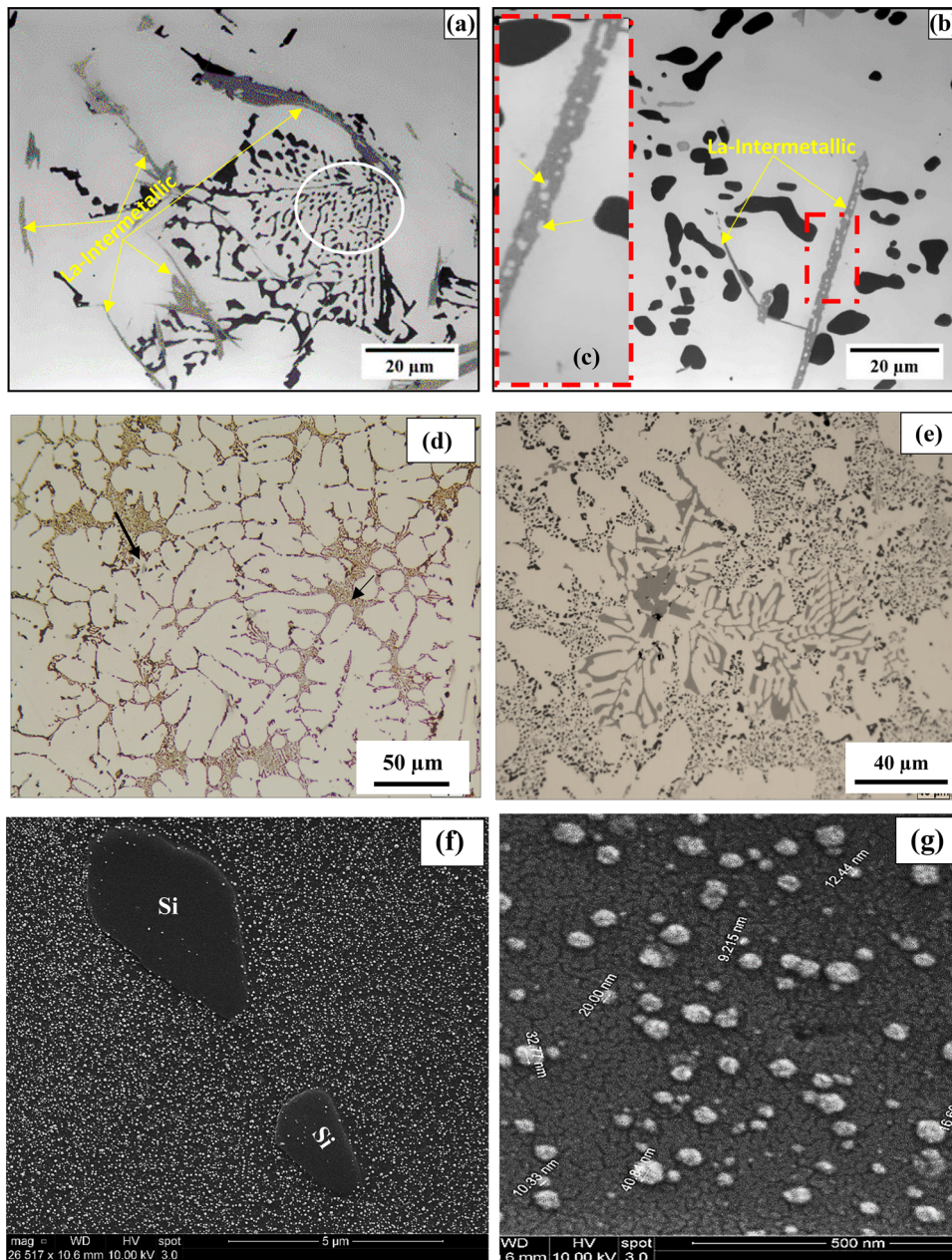
Figure 8. Typical optical microstructures of D00 alloys containing 0.2 wt% La in the: (a) as-cast, (b, c) SHT, (d) alloy D22 modified with 150 ppm Sr-as-cast condition, (e) alloy D22 modified with 150ppm Sr-SHT condition, (f) alloy D00 in the T6 condition, (g) an enlarged area of (f). Note the precipitation of α-Fe within α-Al network in (e). The black arrows in (d) point to the roundness of α-dendrites due to grain refining.

modification with 150 ppm Sr (alloy D22) leads to lowering the UTS, and YS values to 278 MPa and 199 MPa, respectively, with a corresponding increase in ductility from 1.7 to 2.0%. Addition of Ce or La reduces the tensile strength further, to about 210 MPa in the as-cast case, for the different levels of RE addition, whereas the YS level is around 149 MPa. For the 0.2 wt% La addition; however, the reduction in UTS and YS values is approximately 43 MPa and 36 MPa, as demonstrated in Figure 11.

The presence of 0.2 wt% of Ce in the T6-treated D00 alloy leads to enhancing the UTS and YS values of the as-cast D00 base alloy from 300 to 320 MPa and from 240 to 275 MPa, respectively, accompanied by a decrease in the percent elongation from 1.7 to 0.7% as shown in Figure 10. In comparison, Figure 11 reveals that 0.2 wt% addition of La results in UTS and YS values of 374 and 368 MPa, respectively, in the T6-heat-treated alloy, and a ductility of 0.9%. Thus, in T6-treated condition, addition of 0.2 wt% La is much more effective in enhancing the alloy strength
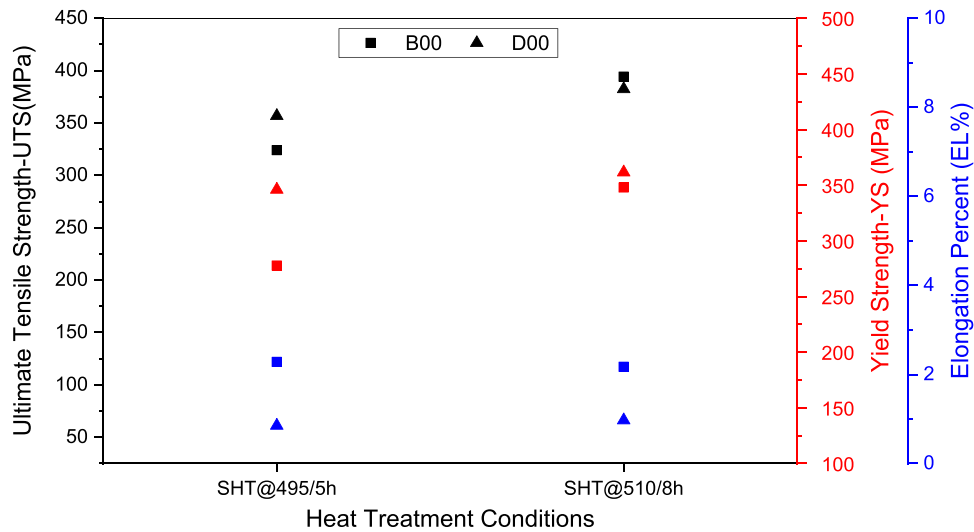
Figure 9. *Effect of solution heat treatment condition on the tensile properties of B00 and D00 alloys.*
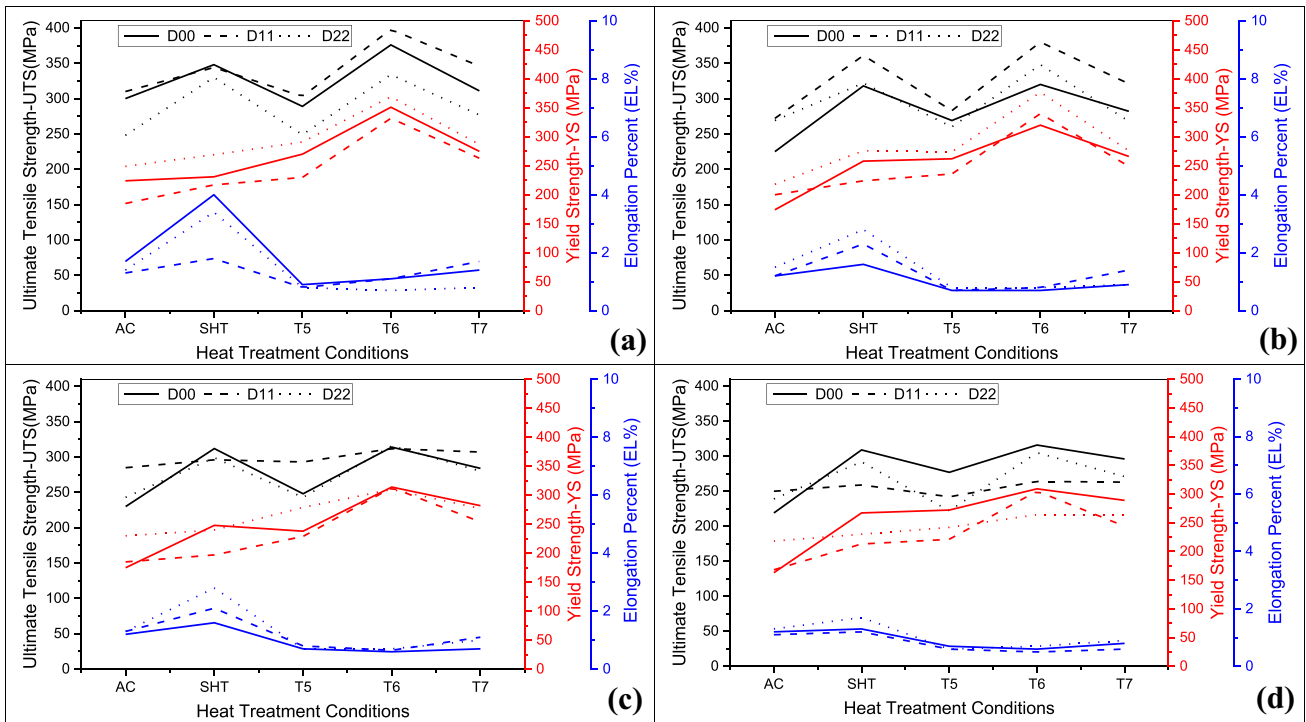

Figure 10. *Average values of ultimate tensile strength (UTS), yield strength (YS) and percent elongation (EL%) obtained from D00 to D22 alloys in the as-cast (AC), T5, T6 and T7 heat-treated conditions (at ambient temperature) with (a) 0.0 wt%, (b) 0.2 wt%, (c) 0.5 wt% and (d) 1.0 wt% addition of Ce.*

compared to 150 ppm Sr addition, while maintaining almost the same ductility at the same time.

Mathematical Analysis

Table 4 lists the tensile properties of the three base alloys in the as-cast condition. Figure 12 exhibits the contribution of the added Ce to the alloy tensile properties in the form of ΔP ($P - P_{\text{ascast}}$) plots where P = UTS, YS or %El (using

the tensile properties of the base alloys in the as-cast condition as a reference), as a function of the applied heat treatment. In this section, the term negative refers to reduction in a certain tensile parameter. It is evident from Figure 12a that addition of RE metals has a negative effect (i.e., reduction) on all alloys in the as-cast condition reaching -80 MPa at 1% RE addition (D00 alloy). Apparently, the presence of other alloying elements in D11 and D22 alloys (Zr, V, Ni, Sr—Table 1) resulted in
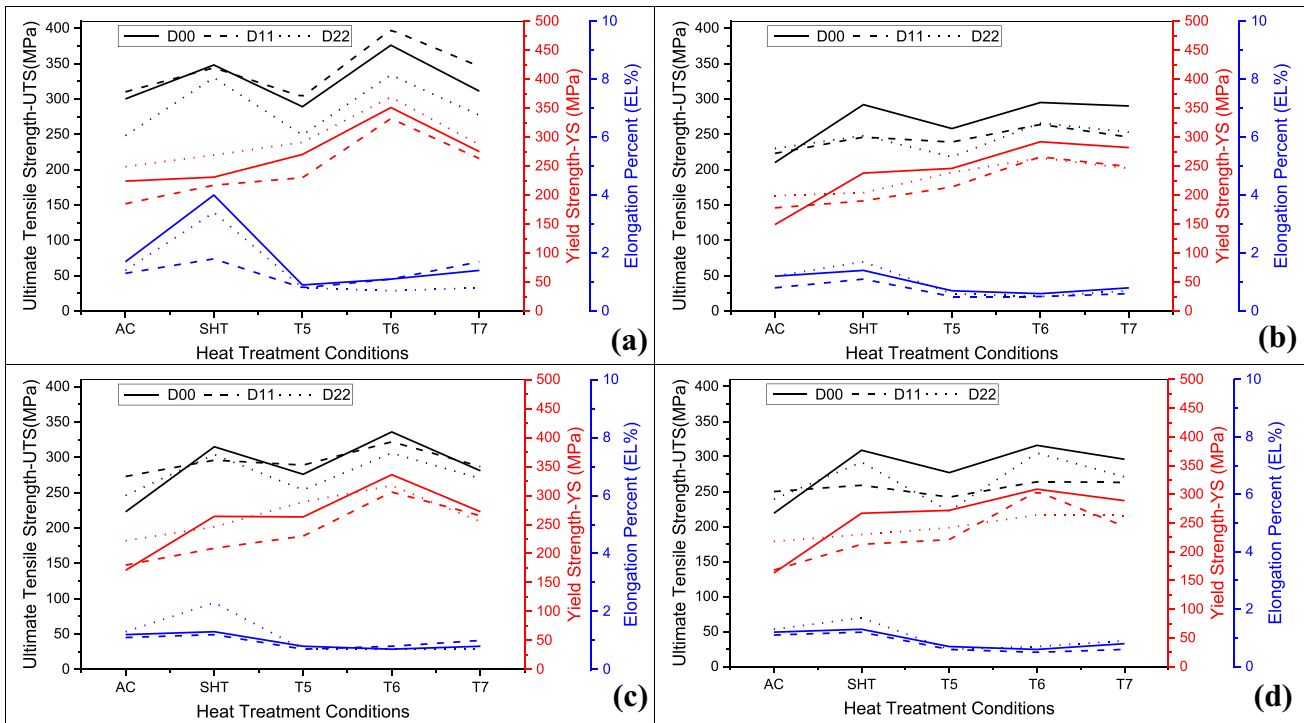
Figure 11. Average values of ultimate tensile strength, yield strength (YS) and elongation percent (EL%) obtained from D00 to D22 alloys in the as-cast(AC), T5, T6 and T7 heat-treated conditions (at ambient temperature) with (a) 0.0 wt%, (b) 0.2 wt%, (c) 0.5 wt% and (d) 1.0 wt% addition of La.

Table 4. Tensile Properties of the Three Base Alloys—Table 1

| Alloy code	UTS, MPa	YS, MPa	%El
D00	300	240	1.75
D11	310	250	1.25
D22	250	180	1.3

compromising the negative effect of Ce addition to some extent. Similar observations are noted for the alloys in the T5 condition.

Solutionizing the alloys at 510 °C for 8 h led to marked improvement in the contribution of Ce when added in small amounts ($\sim$ 0.2%). A part of the observed increase in the UTS levels may be attributed to fragmentation of the eutectic Si particles and hence hardening by the fragments of Si instead of the long sharp edged ones.[75] As shown in Figure 8e, aging the alloys at 180 °C/8 h caused decomposition of the supersaturated matrix resulting in dense precipitation of Al_2Cu particles (10–40 nm) and hence a significant increase in the alloy UTS value without or with 0.2% Ce. Beyond this concentration, the precipitation of RE-based intermetallics negates the beneficial role of precipitation hardening reaching almost nil at 0.5%Ce and − 40MPa at 1%Ce. Increasing the aging temperature to 240 °C (over-aging) with the associated increase in particle

size would lead to improvement in the alloy %El at the cost lowering its YS and UTS levels. In this case, only alloys with Ce up to 0.2% could retain some hardening (40 MPa) with a gradual decrease into the negative side with Ce as high as 1%.

As in the case of UTS, the contribution of Ce to the alloy YS was significantly negative (reduction) in the as-cast condition, with improvement when the alloys were solutionized or treated in T5 condition (as cast + 180 °C/ 8 h)—Figure 12b. The maximum improvement took place after T6 aging for alloys with minimum amount of Ce (0.2%)—almost 150 MPa for D22 alloy that was modified with 150 ppm Sr. Similar observation was made for the T7-treated alloys reaching about 75 MPa in alloys with no Ce. Considering the changes in the alloy ductility, all additions—Ce or transition elements—resulted in decreasing %El except when the alloys with no Ce were solutionized at 510 °C/8 h as shown in Figure 12c.

Figure 13 shows the contribution of La to the strength parameters of the three base alloys. As in case of Ce, addition of RE and the consequent increase in the volume fraction of all types of intermetallics resulted in a marked decrease in the alloys UTS levels in the as-cast and T5 conditions—Figure 13a. Maximum contribution is attributed to either transition metals (0% RE) or with 0.2%La, 80 MPa for SHT and T6 conditions. Beyond this limit, the UTS suffers a significant reduction reaching − 60 MPa with the addition of 1%La. Addition of 0.5% La resulted in almost
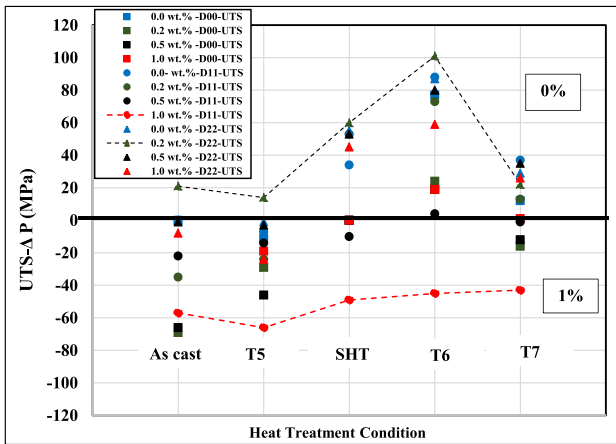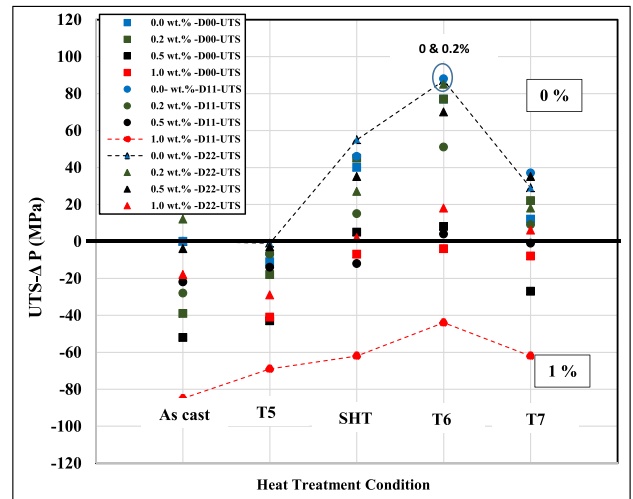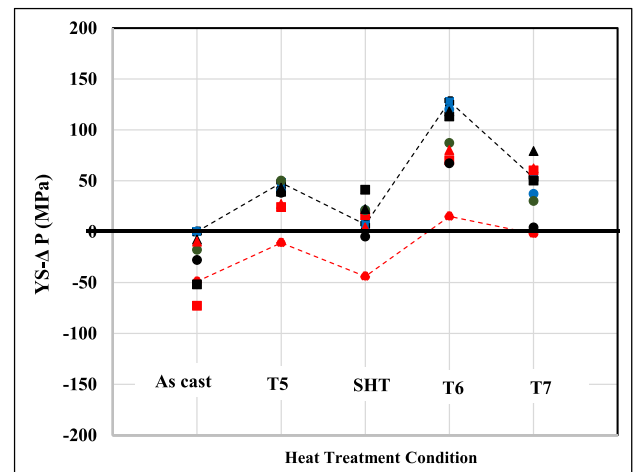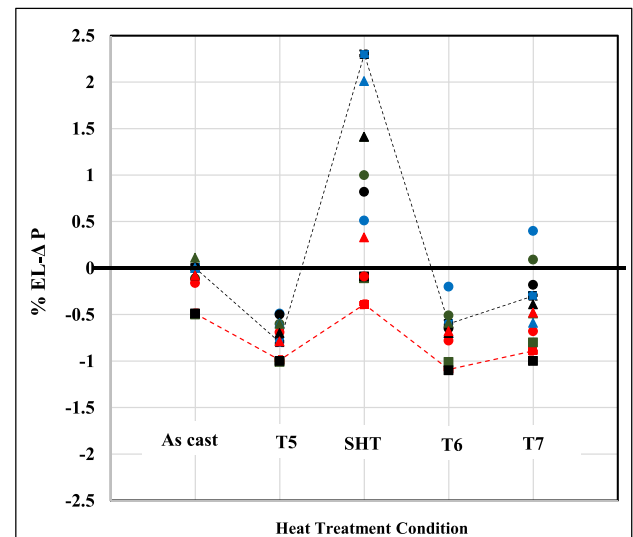
(a)
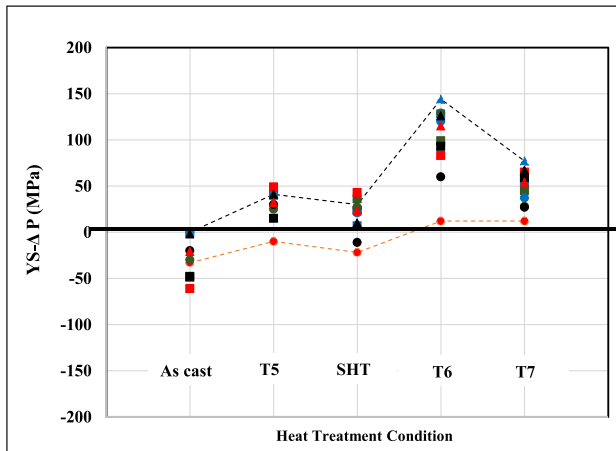
(b)
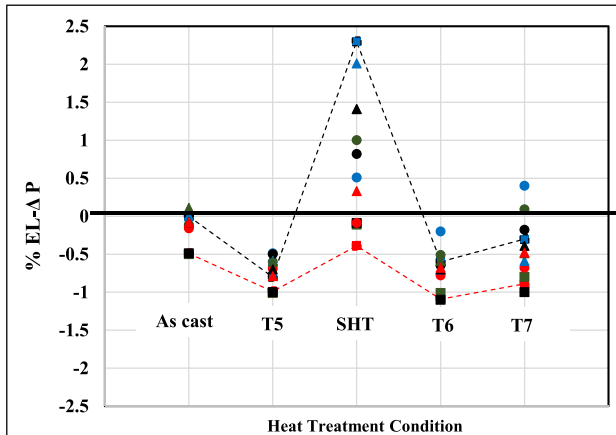
(c)

Figure 12. Effect of added Ce on the tensile properties of alloys D00, D11 and D22 in the as-cast condition; (a) UTS, (b) YS and (c) %El. Legends as in (a). Black and red broken lines indicate 0% Ce and 1% Ce, respectively.

(a)

(b)

(c)

Figure 13. Contribution of added La to: (a) UTS, (b) YS, (c) %El. Legends as in (a). Black and red broken lines indicate 0% La and 1% La, respectively.
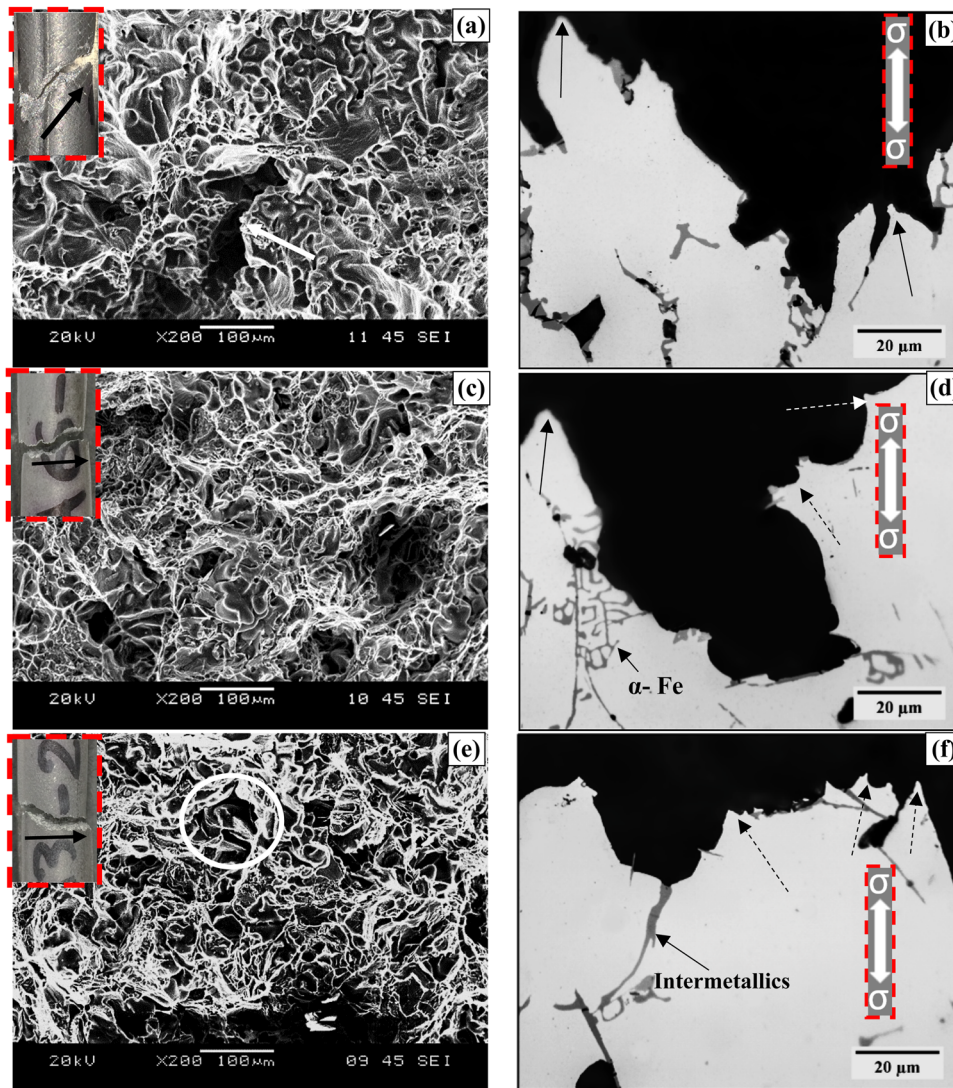
Figure 14. *Tensile fractured microstructures of T6-B00 alloys (a, b) without rare earth addition, (c, d) with 1.0 wt% Ce, and (d, e) with 1.0 wt% La addition, which were observed (a, c, e) perpendicular, and (b, d, f) parallel to the tensile direction. Note the change in the fracture angle in (c) and (e). Note the presence of cleavage in the white circled area in (e).*

complete elimination of the hardening due to precipitation of Al_2Cu particles. Yield strength (Figure 13b) revealed a better response to all alloying elements including La in the T5 and T6 conditions compared to that displayed by the UTS levels. In the T6 condition, alloy D00 achieved 150 MPa increase in the YS level (0 and 0.2%La). Apparently, the use of RE has practically no influence on the alloy strength, in particular in the T6 condition. Figure 13c exhibits the effect of all added elements on their contribution to the alloy ductility. As can be seen, maximum contribution was achieved when D00 and D22 (containing 150 ppm Sr) alloys were solutionized at 510 °C/8 h. With respect to the ductility, all alloys revealed clear reduction in their % elongation values (Figure 13c). Note the similarity between Figures 12c and 13c.

Fractography

Figure 14a exhibits the details of the fracture surface of B00 alloy in the T6 condition where a noticeable void can be seen at the center of the tensile bar (white arrow) surrounded by a network of fine dimples. The inset in the upper left corner of Figure 14a shows the actual fracture angle with respect to the loading axis − 45° shear angle. Due to the absence of both RE and Si, the section beneath Figure 14a reveals stretching of the dendrites in the loading direction (Figure 14b—black arrow). Although the addition of 1% Ce or La did not cause noticeable change in the fracture behavior of the B00 alloy due to the relatively high ductility of the alloy (Figure 14c, e), the longitudinal section beneath the fracture surface revealed a clear decrease
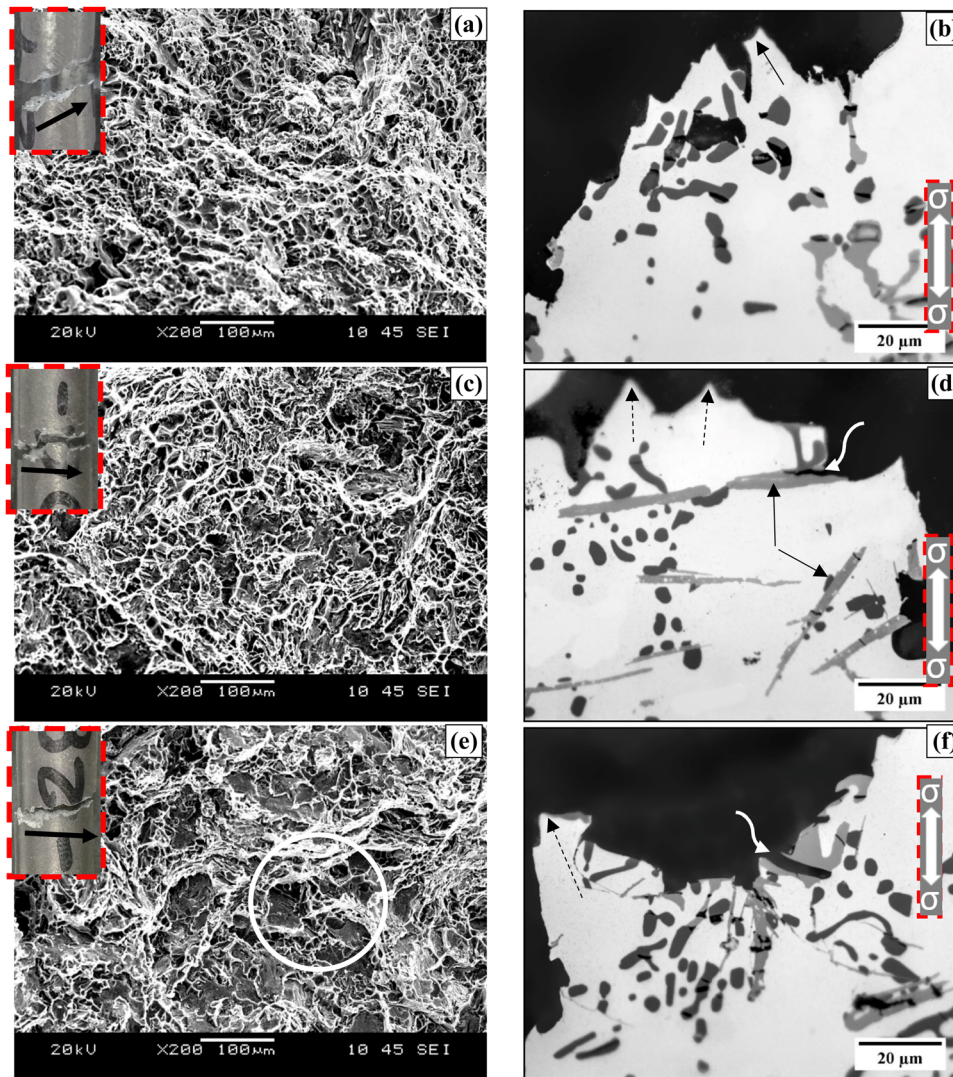
Figure 15. Tensile fractured microstructures of T6-D00 alloy (a, b) without rare earth addition, (c, d) with 1.0 wt% Ce, and (d, e) with 1.0 wt% La addition, which were observed (a, c, e) perpendicular, and (b, d, f) parallel to the tensile direction.

in the stretched dendrites as indicated by broken arrows in Figure 14d, f caused by the decrease in the alloy ductility.

Figure 15 presents the fracture behavior of D00 alloy in the T6 condition and the effect of addition of 1% Ce or La. In all cases, the cracks were confined to the interior on the eutectic Si particles coupled with the presence of a cleavage area in RE-containing alloys (white circled area in Figure 15e), compared to a uniform dimple structure in the base alloy (Figure 15a). Both RE-intermetallics and Si particles acted as crack openers as indicated by the white arrows in Figure 15d, f. As in the case of B00 alloy, the angle between the fracture direction (inset micrographs) and the loading axis changed from 45° to almost 90°, with the increase in the amount of RE-intermetallics.

Figure 16 exhibits a series of backscattered electron images representing the fracture surface of D00 alloy in the T6

condition with 1% of Ce or 1% of La. Ultra-fine particles (similar to those shown in Figure 8d) are visible in all micrographs, in particular as shown in Figure 16a (see red dashed circles), in addition to either Fe-based intermetallics (white circled area in Figure 16a) or RE-based intermetallics as shown in Figure 16b, c. Since Ce and La are having close atomic numbers (57 and 58), it is difficult to distinguish between the micro-constituents in these two figures. Figure 16d is a high-magnification image of the white area in Figure 16a, showing the morphology of the precipitated particles (< 200 nm) that was identified as Al_2Cu from the associated EDS spectrum presented in Figure 16e. As the EDS was generated from a fracture surface, the Cu/Al ratio is not 1/2.
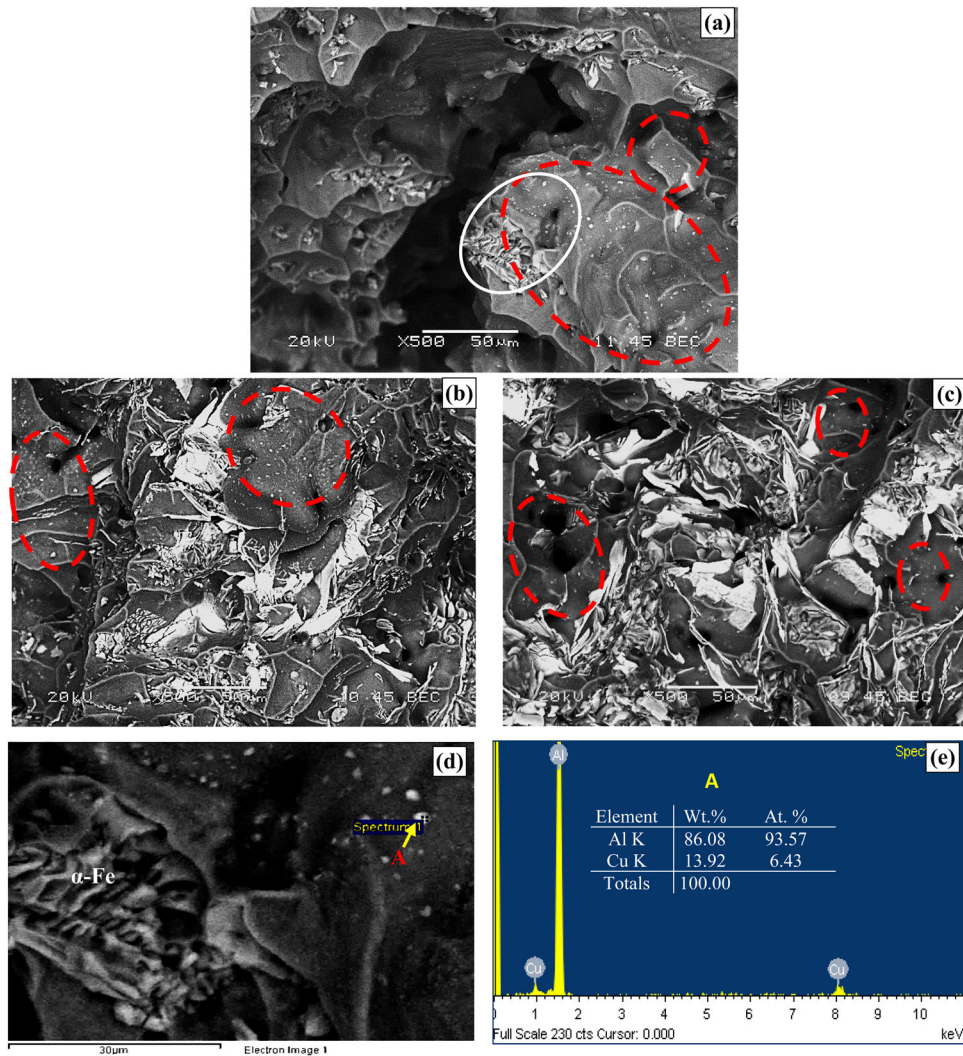
Figure 16. BSE images of the fracture surface of T6-treated D00 alloy with addition of (a) 0.0 wt% RE, (b) 1.0 wt% Ce, and (c) 1.0 wt% La, (d) Enlarged BSE image of the circled area, (e) EDS spectrum from particle A in (d), corresponding Al$_2$Cu precipitation.

Conclusions

Based on the findings documented in the present work, the following conclusions may be drawn:

1. Addition of RE metals (La or Ce) leads to the appearance of exothermic peaks in the solidification and heating curves between the precipitation of the primary α-Al phase and the (Al–Si) eutectic reaction.

2. The magnitude of the exothermic peak corresponding to the Al$_2$Cu and Q-phases is noticeably larger in the base alloy D00 compared to the alloy with 1.0 wt% RE (La/Ce) addition, and is totally absent in the D00 alloy containing 5.0 wt% RE.

3. The morphology of the RE intermetallic phases is based on the RE level of addition, as they appear in the form of spot-type particles in the microstructure with a small amount of RE addition (0.2 wt%), but with coarse block-like and lath-like morphologies when the RE addition increases to 1.0 wt%.

4. Addition of 0.2% RE has a more pronounced effect on the alloy yield strength (15%) than on the ultimate tensile strength (6%) in the as-cast condition.

5. The fracture surface of T6-treated D00 alloy containing 1.0 wt% Ce/La is covered by cleavage planes.

REFERENCES

1. K. Nogita et al., Mechanisms of eutectic solidification in Al–Si alloys modified with Ba, Ca, Y and Yb. J. Light Met. **1**(4), 219–228 (2001)

2. B. Li, F. Kong, Y. Chen, Effect of yttrium addition on microstructures and room temperature tensile properties of Ti–47 Al alloy. J. Rare Earths **24**(3), 352–356 (2006)

3. H.Z. Li et al., Effect of Y content on microstructure and mechanical properties of 2519 aluminum alloy. Trans. Nonferrous Met. Soc. China **17**(6), 1194–1198 (2007)

4. L. Zheng, H. Yongmei, Effect of yttrium on the microstructure of a semi-solid A356 Al alloy. Rare Met. **27**(5), 536–540 (2008)

5. M. Li et al., The effect of Y on the hot-tearing resistance of Al–5wt% Cu based alloy. Mater. Des. **31**(5), 2483–2487 (2010)

6. B. Li et al., Effects of yttrium and heat treatment on the microstructure and tensile properties of Al–7.5 Si–0.5 Mg alloy. Mater. Des. **32**(3), 1617–1622 (2011)

7. J.H. Li, P. Schumacher, Effect of Y addition and cooling rate on refinement of eutectic Si in Al–5 wt% Si alloys. Int, J. Cast Met. Res. **25**(6), 347–357 (2012)

8. B. Wan et al., Effect of trace yttrium addition on the microstructure and tensile properties of recycled Al–7Si–0.3 Mg–1.0 Fe casting alloys. Mater. Sci. Eng. A **666**, 165–175 (2016)

9. M.O. Shabani, A. Mazahery, Automotive copper and magnesium containing cast aluminium alloys: report on the correlation between Yttrium modified microstructure and mechanical properties. Russ. J. Non-Ferrous Met. **55**(5), 436–442 (2014)

10. M. Sheng et al., Effects of Y and Y combined with Al-5Ti-1B on the microstructure and mechanical properties of hypoeutectic Al–Si alloy. JOM **67**(2), 330–335 (2015)

11. Z.R. Nie, et al. Research on rare earth in aluminum. In *Materials Science Forum* (Trans Tech Publ., 2002)

12. Z. Nie, et al. Advanced aluminum alloys containing rare-earth erbium. In *Materials Forum* (2004)

13. G.F. Xu et al., Effect of trace rare earth element Er on Al–Zn–Mg alloy. Trans. Nonferrous Met. Soc. China **16**(3), 598–603 (2006)

14. Y.T. Li, et al. Alloying behavior of rare-earth Er in Al–Cu–Mg–Ag alloy. In *Materials Science Forum* (Trans Tech Publ., 2007)

15. S.P. Wen et al., The effect of erbium on the microstructure and mechanical properties of Al–Mg–Mn–Zr alloy. Mater. Sci. Eng. A Struct. Mater. Prop. Microstruct. Process. **516**(1–2), 42–49 (2009)

16. K. Nogita et al., The role of trace element segregation in the eutectic modification of hypoeutectic Al–Si alloys. J. Alloys Compd. **489**(2), 415–420 (2010)

17. X. Pengfei et al., Effect of erbium on properties and microstructure of Al–Si eutectic alloy. J. Rare Earths **28**(6), 927–930 (2010)

18. C. Booth-Morrison, D.N. Seidman, D.C. Dunand, Effect of Er additions on ambient and high-temperature strength of precipitation-strengthened Al-Zr-Sc-Si alloys. Acta Materialia **60**(8), 3643–3654 (2012)

19. X.W. Hu et al., Effects of rare earth Er additions on microstructure development and mechanical properties of die-cast ADC12 aluminum alloy. J. Alloys Compd. **538**, 21–27 (2012)

20. X.D. Wang et al., Microstructure and mechanical properties of Al-Mg-Mn alloy with erbium. Rare Met. **31**(3), 237–243 (2012)

21. Z.M. Shi et al., Effects of erbium modification on the microstructure and mechanical properties of A356 aluminum alloys. Mater. Sci. Eng. A Struct. Mater. Prop. Microstruct. Process. **626**, 102–107 (2015)

22. M. Colombo, E. Gariboldi, A. Morri, Er addition to Al-Si-Mg-based casting alloy: Effects on microstructure, room and high temperature mechanical properties. Journal of Alloys and Compounds **708**, 1234–1244 (2017)

23. M. Colombo, E. Gariboldi, A. Morri, Influences of different Zr additions on the microstructure, room and high temperature mechanical properties of an Al–7Si–0.4 Mg alloy modified with 0.25% Er. Mater. Sci. Eng. A **713**, 151–160 (2017)

24. Q.L. Li, et al. Effect of rare earth Er on microstructure and mechanical properties of cast Al–Si–Mg alloy. In *Materials Science Forum* 35. (Trans Tech Publ., 2017)

25. C. Xu et al., Effect of Al–P–Ti–TiC–Nd$_2$O$_3$ modifier on the microstructure and mechanical properties of hypereutectic Al–20wt% Si alloy. Mater. Sci. Eng. A **452**, 341–346 (2007)

26. W.X. Shi et al., Effect of Nd on microstructure and wear resistance of hypereutectic Al–20% Si alloy. J. Alloys Compd. **508**(2), 480–485 (2010)

27. S. Weixi et al., Effect of neodymium on primary silicon and mechanical properties of hypereutectic Al–15% Si alloy. J. Rare Earths **28**, 367–370 (2010)

28. X. Ren et al., Effect of Nd on microstructure and properties of 2A70 alloy. J. Alloys Compd. **731**, 1014–1021 (2017)

29. Q. Tang et al., The effects of neodymium addition on the intermetallic microstructure and mechanical properties of Al–7Si–0.3 Mg–0.3 Fe alloys. J. Alloys Compd. **741**, 161–173 (2018)

30. R. Ahmad, M. Asmael, M. Amzar, Effect of ytterbium addition on microstructure and hardness of Al–6.5Si–1Zn secondary cast alloy. J. Eng. Appl. Sci. **11**(16), 10123–10127 (2006)

31. D. Xiao et al., Effect of rare earth Yb addition on mechanical properties of Al–5· 3Cu–0· 8Mg–0· 6Ag alloy. Mater. Sci. Technol. **23**(10), 1156–1160 (2007)

32. X.M. Zhang et al., Effects of Yb addition on microstructures and mechanical properties of 2519A aluminum alloy plate. Trans. Nonferrous Met. Soc. China **20**(5), 727–731 (2010)

33. B. Li et al., Microstructure evolution and modification mechanism of the ytterbium modified Al–7.5%Si–0.45%Mg alloys. J. Alloys Compd. **509**(7), 3387–3392 (2011)

34. J.H. Li et al., Refinement of eutectic Si phase in Al–5Si alloys with Yb additions. Metall. Mater. Trans. A Phys. Metall. Mater. Sci. **44a**(2), 669–681 (2013)

35. Z. Hu et al., Solidification behavior, microstructure and silicon twinning of Al–10Si alloys with Yb addition. J. Rare Earths **36**, 662–668 (2018)

36. Q. Li et al., Mechanical properties and microstructural evolution of Yb-modified Al–20% Si alloy. J. Mater. Eng. Perform. **27**, 3498–3507 (2018)

37. K. Nogita, S.D. McDonald, A.K. Dahle, Eutectic modification of Al–Si alloys with rare earth metals. Mater. Trans. **45**(2), 323–326 (2004)

38. Z.W. Chen, P. Chen, C.Y. Ma, Microstructures and mechanical properties of Al–Cu–Mn alloy with La and Sm addition. Rare Met. **31**(4), 332–335 (2012)

39. H. Qiu, H. Yan, Z. Hu, Effect of samarium (Sm) addition on the microstructures and mechanical properties of Al–7Si–0.7 Mg alloys. J. Alloys Compd. **567**, 77–81 (2013)

40. R. Yuansheng, Y. Hong, H. Zhi, Modification of eutectic silicon and β-Al 5 FeSi phases in as-cast ADC12 alloys by using samarium addition. J. Rare Earths **31**(9), 916–922 (2013)

41. H. Zhi, Y. Hong, Y. Rao, Effects of samarium addition on microstructure and mechanical properties of as-cast Al-Si-Cu alloy. Trans. Nonferrous Met. Soc. China **23**(11), 3228–3234 (2013)

42. H.X. Qiu, H. Yan, Z. Hu, Modification of near-eutectic Al–Si alloys with rare earth element samarium. J. Mater. Res. **29**(11), 1270–1277 (2014)

43. Q. Li et al., Effect of samarium (Sm) addition on the microstructure and tensile properties of Al–20% Si casting alloy. Int. J. Metalcast. **12**, 554–564 (2017)

44. V.V. Zakharov, T.D. Rostova, Effect of scandium, transition metals, and admixtures on strengthening of aluminum alloys due to decomposition of the solid solution. Met. Sci. Heat Treat. **49**(9–10), 435–442 (2007)

45. M.S. Kaiser et al., Effect of scandium on the microstructure and ageing behaviour of cast Al–6Mg alloy. Mater. Charact. **59**(11), 1661–1666 (2008)

46. W. Prukkanon, N. Srisukhumbowornchai, C. Limmaneevichitr, Influence of Sc modification on the fluidity of an A356 aluminum alloy. J. Alloys Compd. **487**(1–2), 453–457 (2009)

47. D. Emadi, A.K.P. Rao, M. Mahfoud, Influence of scandium on the microstructure and mechanical properties of A319 alloy. Mater. Sci. Eng. A Struct. Mater. Prop. Microstruct. Process. **527**(23), 6123–6132 (2010)

48. W. Zhang et al., Effects of Sc content on the microstructure of As-Cast Al-7wt.% Si alloys. Mater. Charact. **66**, 104–110 (2012)

49. U. Patakham, J. Kajornchaiyakul, C. Limmaneevichitr, Modification mechanism of eutectic silicon in Al–6Si–0.3 Mg alloy with scandium. J. Alloys Compd. **575**, 273–284 (2013)

50. M. Yi, Z.-H. Zhao, J.-Z. Cui, Effect of minor Zr and Sc on microstructures and mechanical properties of Al–Mg–Si–Cu–Cr–V alloys. Trans. Nonferrous Met. Soc. China **23**(7), 1882–1889 (2013)

51. J. Ma et al., Effect of Sc addition on microstructure and mechanical properties of 1460 alloy. Prog. Nat. Sci. Mater. Int. **24**(1), 13–18 (2014)

52. Y.-C. Tzeng et al., Effects of scandium addition on iron-bearing phases and tensile properties of Al–7Si–0.6 Mg alloys. Mater. Sci. Eng. A **593**, 103–110 (2014)

53. C. Xu et al., The synergic effects of Sc and Zr on the microstructure and mechanical properties of Al–Si–Mg alloy. Mater. Des. **88**, 485–492 (2015)

54. J.H. Li et al., Modification of eutectic Si in Al–Si alloys with Eu addition. Acta Mater. **84**, 153–163 (2015)

55. F. Mao et al., The interaction between Eu and P in high purity Al–7Si alloys. Mater. Charact. **120**, 129–142 (2016)

56. F. Mao et al., Effect of Eu addition on the microstructures and mechanical properties of A356 aluminum alloys. J. Alloys Compds. **650**, 896–906 (2015)

57. W.Y. Liu et al., Synergistic effects of Gd and Zr on grain refinement and eutectic Si modification of Al–Si cast alloy. Mater. Sci. Eng. A Struct. Mater. Prop. Microstruct. Process. **693**, 93–100 (2017)

58. O. El Sebaie, *The Effect of Mischmetal, Cooling Rate and Heat Treatment on the Microstructure and Hardness of 319, 356, and 413 Aluminum-Silicon Alloys* (UQAC, 2006)

59. O. El Sebaie et al., The effects of mischmetal, cooling rate and heat treatment on the hardness of A319.1, A356.2 and A413.1 Al–Si casting alloys. Mater. Sci. Eng. A. **486**(1), 241–252 (2008)

60. O. El Sebaie et al., The effects of mischmetal, cooling rate and heat treatment on the eutectic Si particle characteristics of A319.1, A356.2 and A413.1 Al–Si casting alloys. Mater. Sci. Eng. A **480**(1–2), 342–355 (2008)

61. O. Elsebaie, F.H. Samuel, S. Al Kahtani, Intermetallic phases observed in non-modified and Sr-modified Al–Si cast alloys containing mischmetal. Int. J. Cast Met. Res. **26**(1), 1–15 (2013)

62. G.S. Mousavi, M. Emamy, J. Rassizadehghani, The effect of mischmetal and heat treatment on the microstructure and tensile properties of A357 Al–Si casting alloy. Mater. Sci. Eng. A Struct. Mater. Prop. Microstruct. Process. **556**, 573–581 (2012)

63. Z.Y. Ouyang, X.M. Mao, M. Hong, Multiplex modification with rare earth elements and P for

hypereutectic Al–Si alloys. J. Shanghai Univ. (Engl. Ed.) **11**, 400–402 (2007)

64. Y.C. Tsai et al., Effect of trace La addition on the microstructures and mechanical properties of A356 (Al–7Si–0.35 Mg) aluminum alloys. J. Alloys Compd. **487**(1), 157–162 (2009)

65. S.A. Alkahtani et al., Effect of rare earth metals on the microstructure of Al–Si based alloys. Materials (Basel) **9**(1), 45 (2016)

66. E. Elgallad et al., Microstructural characterisation of Al–Si cast alloys containing rare earth additions. Philos. Mag. **98**, 1337–1359 (2018)

67. E.M. Elgallad et al., Effects of La and Ce Addition on the Modification of Al-Si Based Alloys. Adv. Mater. Sci. Eng. (2016). https://doi.org/10.1155/2016/5027243

68. M.G. Mahmoud et al., Effect of solidification rate and rare earth metal addition on the microstructural characteristics and porosity formation in A356 alloy. Adv. Mater. Sci. Eng. (2017). https://doi.org/10.1155/2017/5086418

69. M.G. Mahmoud et al., Effect of rare earth metals, Sr, and Ti addition on the microstructural characterization of A4131 alloy. Adv. Mater. Sci. Eng. (2017). https://doi.org/10.1155/2017/4712946

70. A.M. Nabawy et al., Role of cerium, lanthanum, and strontium additions in an Al–Si–Mg (A356) alloy. Int. J. Mater. Res. **107**(5), 446–458 (2016)

71. A.M. Samuel et al., Intermetallic precipitation in rare earth-treated A413.1 alloy: a metallographic study. Int. J. Mater. Res. **109**(2), 157–171 (2018)

72. *Global Supplier of Fabricated Products & Machining Parts | Stanford Advanced Materials*. 2018. http://www.samaterials.com/.

73. L. Backerud, G. Chai, J. Tamminen, *Solidification Characteristics of Aluminum Alloys, Foundry Alloys*, vol. 2 (American Foundrymens Society Inc, 1990), p. 266

74. H.K. Yi, D. Zhang, Modification effect of pure rare earth metal La on as—cast hypereutectic Al—17% Si alloys. China Nonferrous Met. Soc. J. **13**(2), 358–364 (2003)

75. M. Ibrahim, M. Abdelaziz, A.M. Samuel, H. Doty, F.H. Samuel, Spheroidization and coarsening of eutectic Si particles in Al–Si-based alloys. Adv. Mater. Sci. Eng. (2021). https://doi.org/10.1155/2021/6678280